nature communications

Article

https://doi.org/10.1038/s41467-024-54759-0

Transcranial optogenetic brain modulator for precise bimodal neuromodulation in multiple brain regions

Received: 27 March 2023

Accepted: 18 November 2024

Published online: 30 November 2024

Check for updates

Hyogeun Shin[1], Min-Ho Nam[2], Seung Eun Lee[3], Soo Hyun Yang[4,5], Esther Yang[4,5], Jin Taek Jung[4,5], Hyun Kim[4,5], Jiwan Woo[3], Yakdol Cho[3], Youngsam Yoon[6] & Il-Joo Cho[4,5,7]

Transcranial brain stimulation is a promising technology for safe modulation of brain function without invasive procedures. Recent advances in transcranial optogenetic techniques with external light sources, using upconversion particles and highly sensitive opsins, have shown promise for precise neuromodulation with improved spatial resolution in deeper brain regions. However, these methods have not yet been used to selectively excite or inhibit specific neural populations in multiple brain regions. In this study, we created a wireless transcranial optogenetic brain modulator that combines highly sensitive opsins and upconversion particles and allows for precise bimodal neuromodulation of multiple brain regions without optical crosstalk. We demonstrate the feasibility of our approach in freely behaving mice. Furthermore, we demonstrate its usefulness in studies of complex behaviors and brain dysfunction by controlling extorting behavior in mice in food competition tests and alleviating the symptoms of Parkinson's disease. Our approach has potential applications in the study of neural circuits and development of treatments for various brain disorders.

Transcranial brain stimulation (TBS) has received significant attention as a technology that can treat brain diseases and improve brain function, owing to its safety and few side effects[1–4]. Specifically, prominent noninvasive brain stimulation technologies, such as transcranial magnetic stimulation (TMS), transcranial direct current stimulation (tDCS), and transcranial near-infrared stimulation (tNIRS), have been widely used as clinical tools for treating brain diseases[4–6]. However, most TBS techniques suffer from poor spatial resolution due to the spread of stimulation signals and nonspecific stimulation across different cell types, which makes precise neuromodulation difficult and may result in side effects[1]. To overcome these limitations, several transcranial optogenetic neuromodulation techniques have recently been developed[7–12]. In general, optogenetics allows cell type-specific activation or inhibition using photosensitive opsins[13,14]. These opsins are typically delivered to target neurons via viral vectors, which necessitates a craniotomy to enable the virus to infect specific brain regions. Once the opsins are expressed, light must be delivered to the target region using an implanted fiber, light-emitting diode (LED), or waveguide-based implant to excite or inhibit opsin-tagged neurons.

Highly sensitive opsins and upconversion particles (UCPs) have recently been introduced for transcranial optogenetics. The opsins allow transcranial neuromodulation of the mouse brain, despite the

[1]School of Electronic and Electrical Engineering, College of IT Engineering, Kyungpook National University, Daegu, Republic of Korea. [2]Center for Brain Function, Brain Science Institute, Korea Institute of Science and Technology (KIST), Seoul, Republic of Korea. [3]Research Animal Resources Center, Research Resources Division, Korea Institute of Science and Technology (KIST), Seoul, Republic of Korea. [4]Department of Biomedical Sciences, College of Medicine, Korea University, Seoul, Republic of Korea. [5]Department of Anatomy, College of Medicine, Korea University, Seoul, Republic of Korea. [6]Department of Electrical Engineering, Korea Military Academy, Seoul, Republic of Korea. [7]Department of Convergence Medicine, College of Medicine, Korea University, Seoul, Republic of Korea. e-mail: ijcho@korea.ac.kr

scattering and absorption of visible light in the brain tissue[7–10]. UCPs emit visible light by near-infrared (NIR) excitation with low scattering and absorption of light in tissues[11,12]. Although viral and UCP injections via craniotomy are similar to traditional optogenetic techniques, the key difference in transcranial optogenetic neuromodulation is that subsequent light delivery is performed extracranially. Following the initial viral and UCP injections, neural activity can be continuously modulated using only external light sources, eliminating the need for invasive implants.

The recent development of trichromatic UCPs with excitation-specific luminescence has allowed for the selective activation of various types of cells[12]. However, these studies were performed in an environment that transmitted light to the entire chamber in which the animal was located, making it difficult to selectively modulate multiple brain regions (i.e., multi-site optogenetic neuromodulation). Bimodal neuromodulation (i.e., selectively exciting or inhibiting specific neural populations) is challenging but essential for the diverse interrogation of neural circuits. To achieve accurate and diverse modulation of neural circuits, invasive devices (e.g., fibers, micro-LED probes, and OLED probes, referring to organic light-emitting diode probes) have been developed for multi-site[15–19] or bimodal optogenetic neuromodulation[20]. However, their invasiveness induces significant tissue damage, which prevents long-term use. Therefore, the development of a transcranial optogenetic technique with bimodal neuromodulation capability across multiple sites is crucial for precise and diverse modulation of neural circuits in animals while minimizing tissue damage.

To address these challenges, this study presents a synergistic strategy by combining highly sensitive opsins and UCPs with wireless optoelectronic devices, resulting in transcranial and precise brain modulation with multi-site and bimodal optogenetic neuromodulation. To transcranially activate or inhibit the same group of neurons, we co-expressed two different opsins (ReaChR and stGtACR2) that induce cell depolarization of the same neurons using red light (i.e., activation) and cell hyperpolarization using blue light (i.e., inhibition) (Supplementary Fig. 1). For one of the two opsins, we selected the highly photosensitive opsin (ReaChR) because the efficacy of transcranial stimulation by red light was confirmed in a previous study[7]. In addition, we applied a UCP with blue emission to transcranially activate another opsin (stGtACR2) using NIR light[21]. Furthermore, we successfully developed and utilized a wireless optoelectronic device featuring a small LED array that can deliver two wavelengths (red and NIR light) to multiple brain regions in freely behaving mice. In summary, our method enables the transcranial and selective activation of neurons in multiple brain regions using red light and inhibition using NIR light (Fig. 1 and Supplementary Table 1). We demonstrated the ability of the device to perform multi-site bimodal neuromodulation in mice in open-field and closed-tube tests and showed its applicability in complex behavior studies through the control of extortion behavior in a food competition test. Additionally, we verified its potential for treating neurological disorders by reducing behavioral deficits in a mouse model of Parkinson's disease induced by MPTP (1-methyl-4-phenyl-1,2,3,6-tetrahydropyridine). We believe that our strategy has the potential to be

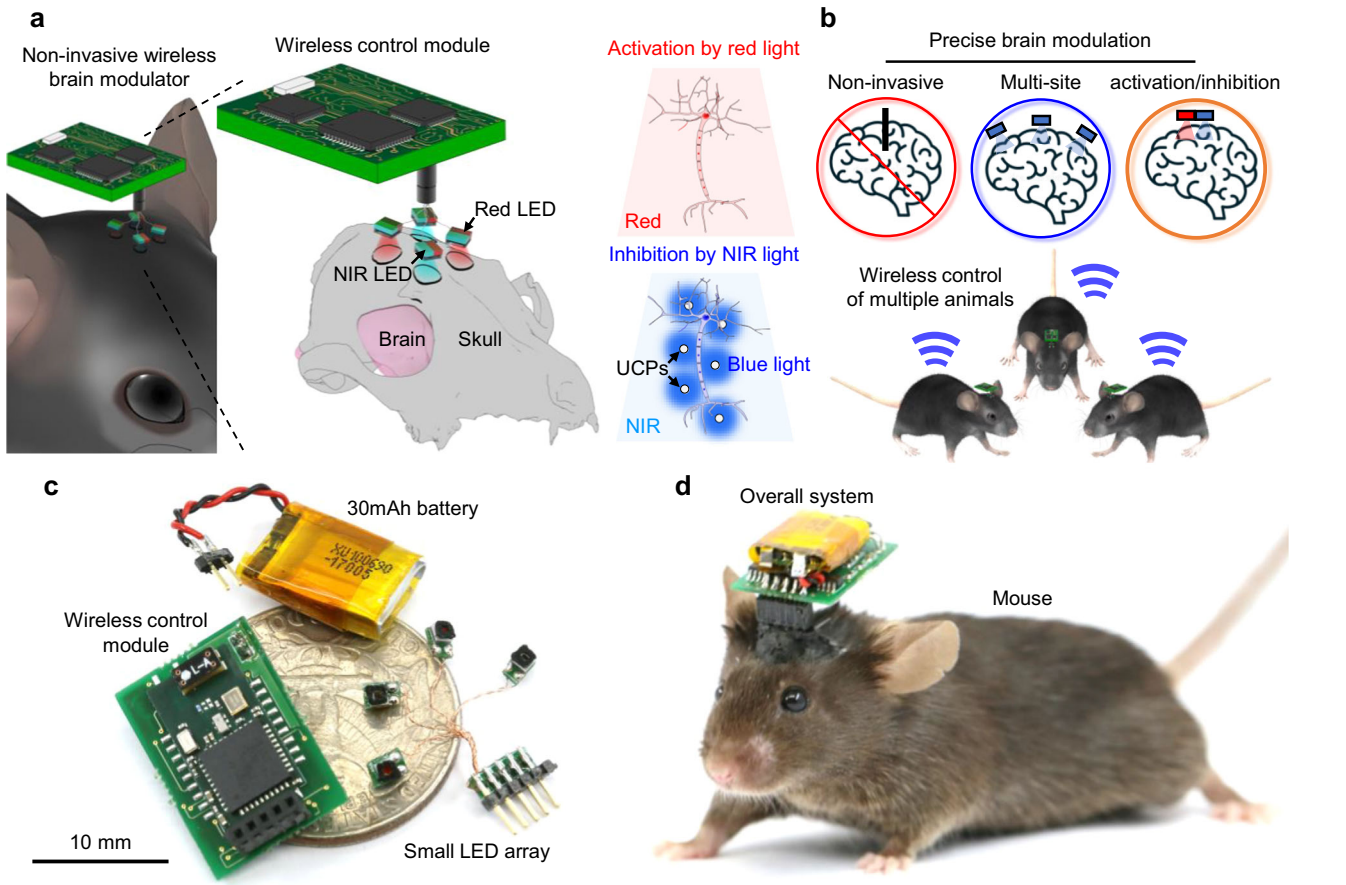

Fig. 1 | Design and features of the transcranial optogenetic brain modulator for precise neuromodulation. a Schematic illustrations of the transcranial brain modulator and its capabilities for multiple-site and bimodal neuromodulation. **b** Schematic illustrations of the features of the transcranial brain modulator. This device enables transcranial, multi-site, and bimodal neuromodulation in multiple animals to precisely modulate brain activity. **c** Photograph showing the overall configuration of the optoelectronic system. **d** Photograph showing the optoelectronic system mounted on the head of a mouse.

a valuable tool for treating neurological disorders caused by dysfunctions in multiple brain regions.

Results

Design and fabrication of wirelessly operated transcranial brain modulator

To achieve transcranial bimodal neuromodulation, two highly sensitive opsins with distinct wavelengths and UCPs were used simultaneously. The two opsins (ReaChR and stGtACR2) depolarize or hyperpolarize neuronal membrane using red or blue light, respectively (λ_{max} = 617 nm (ReaChR[7]), λ_{max} = 480 nm (stGtACR2[22])) (Supplementary Fig. 1). The highly sensitive ReaChR opsin enables activation through red-light delivery outside the skull, resulting in transcranial neuromodulation[7]. To transcranially activate the stGtACR2 opsin as well, we used a UCP that emits visible (NIR) light. We utilized a combination of stGtACR2[22] and a blue-emitting lanthanide particle[21], thus enabling the selective activation of both opsins via transcranial light delivery through the transmission of red and NIR light outside the skull.

We developed a wireless optoelectronic device to transcranially activate the two opsins. The device has several key advantages, including 1) bimodal neuromodulation using high-power, dual-color (Red and NIR) LEDs; 2) multi-site stimulation using an array of four LEDs, each with a small size of 1.6 mm × 1.6 mm; 3) smartphone-controlled wireless operation; 4) a lightweight design that allows the mice to move freely; and 5) Bluetooth wireless communication that allows for selective or simultaneous control of multiple animals without interference. The total weight of the system (four dual-color LED arrays (0.1 g), wireless control module (0.9 g), and 30 mAh battery (0.9 g)) is 1.9 g, which does not affect the behavior of the mice (Supplementary Movie 1, Supplementary Table 1, and Supplementary Fig. 2). To deliver sufficient light to specific brain regions from outside the skull, we chose 1 W high-power red and NIR LEDs with active areas of 1 mm^2 and 0.5625 mm^2, respectively (the packaging process of the LED array is described in the Methods section). The wireless control module, which is designed to control each LED, includes pulse width and frequency modulation capabilities. It features a low-power Bluetooth embedded chip with a microcontroller unit for wireless control, an oscillator integrated circuit (IC) for controlling the LED on/off time, switch ICs for selecting the on/off time, and a p-channel metal-oxide-semiconductor field-effect transient (MOSFET) for a stable supply of high power to the LEDs (Supplementary Fig. 3). This module enables control over the LED selection, stimulation frequency (1 Hz or 10 Hz), and on-time (5 ms or 10 ms) through an Android-based smartphone application (Supplementary Fig. 4; details of the wireless control module are provided in the Methods section). In the behavioral experiments, we primarily used a modulation pattern of 10 Hz with an ON time of 10 ms. This pattern was selected based on previous behavioral studies, including the open field test[23], preference/aversion tests[24], and closed-tube tests[25], which commonly employ frequencies between 5 and 20 Hz to effectively induce behavioral changes. Specifically, increasing the stimulation frequency (5 and 100 Hz) in the closed-tube test led to more pronounced behavioral changes[25]. Thus, we selected 10 Hz, as it represents a midpoint within this range, balancing efficacy and minimizing heat accumulation from the LEDs.

Additionally, we assessed the operating duration of the system using a fully charged 30 mAh battery. The red and NIR LEDs were operated for approximately 53 min each. However, when both the LEDs were operated simultaneously, the battery life decreased to approximately 26 min. Consequently, the high-power consumption of LEDs limited their operating time to approximately 1 h, which decreased further when multiple LEDs were used concurrently. An operating time of approximately 1 h is sufficient for conducting short-term behavioral experiments[25–27].

To further investigate the feasibility of bimodal neuromodulation using different combinations of viruses, UCPs, and LEDs, we analyzed the overlapping spectra of each component (Supplementary Fig. 5). Our analysis showed no overlap between the emission wavelength of the Red LED and the response wavelength of stGtACR2 (Supplementary Fig. 5b); however, there was a significant overlap with the response wavelength of ReaChR (Supplementary Fig. 5b). This indicates that neuronal activation via ReaChR using the Red LED is feasible. Additionally, the emission wavelength of the Blue UCP generated by the NIR-Blue UCP combination overlaps with the response and peak wavelengths of stGtACR2 (Supplementary Fig. 5c). However, the response of ReaChR to the NIR-Blue UCP combination was approximately 60% of that of stGtACR2, enabling selective neuronal inhibition through stGtACR2. Furthermore, the Green UCP exhibited a narrow emission spectrum with a peak at 550 nm, and the response efficiency of ReaChR was substantially higher than that of stGtACR2 (Supplementary Fig. 5d). Thus, to control neural activity in deep brain regions, we used blue and green UCPs to selectively activate ReaChR and stGtACR2, respectively. Overall, these results confirm that bimodal neuromodulation is feasible using various combinations based on the spectral overlap analysis.

In conclusion, by integrating a combination of opsins and particles, our system can provide transcranial, multi-site, and bimodal neuromodulation in freely behaving small animals.

Thermal effects of LED operation

To evaluate the potential for tissue damage by heat from LED operation, we measured the surface temperature of the LEDs and estimated the corresponding temperature increase in the brain tissue (Supplementary Table 2 and Supplementary Fig. 6). During continuous operation, the LED temperature rapidly increased, reaching a maximum of 77.9 °C for the Red LED and 88.1 °C for the NIR LED due to overheating (Supplementary Fig. 6b). However, when operated with a 10% duty cycle, the LEDs maintained stable temperatures of 37 °C for the Red LED and 39.1 °C for the NIR LED, aided by adequate cooling (Supplementary Fig. 6c). In addition, we attached a plastic-based thermal isolator to limit light dispersion and measured the temperature at the end. Under the 10% duty cycle with the thermal isolator attached, during 10 minutes of operation, the maximum temperatures were 34.5 °C for the Red LED and 36.8 °C for the NIR LED (Supplementary Fig. 6d). These temperatures are below body temperature (37 °C), indicating that the heat from the LED is unlikely to cause brain damage.

However, operating the NIR LED at 10% duty cycle without the thermal isolator resulted in temperatures exceeding 39 °C, which could potentially cause brain damage[28]. Using Fourier's Law of heat conduction, we calculated the temperature change across the skull and found that the heat transferred to the brain could exceed 39 °C, indicating a risk of brain damage with prolonged exposure (Supplementary Note 1).

These results suggest that under specific conditions (LED with thermal isolator, 10% duty cycle), the potential for thermal stimulation or cell damage due to LED operation is low.

Transcranial optogenetic modulation of neurons in vivo

The initial objective of our study was to evaluate the feasibility of our optogenetic strategy in animals by determining the efficacy of transcranial modulation and the stimulation depth, which is dependent on the combination of the virus, LED, and particles (e.g., stGtACR2–NIR–Blue UCP) in vivo. To achieve this goal, we conducted electrophysiology experiments using three combinations (ReaChR–Red LED, ReaChR–NIR LED–Green UCP, and stGtACR2–NIR LED–Blue UCP) (Supplementary Fig. 7) (The detailed experimental protocol, including surgery and experimental setup, is provided in the Methods section). After injecting viruses and particles into various

brain regions (cortex, hippocampus, and thalamus) (Supplementary Fig. 7), we allowed four weeks for sufficient infection. We then inserted a neural probe with 16 black platinum microelectrodes into the infected regions of each mouse (Supplementary Fig. 7).

In the first experiment, we measured neural activation using red light on the skull of a mouse infected with the ReaChR virus. In the sensory cortex region, we successfully observed a statistically significant increase in neural signals with red light illumination at 63 mW·mm^{-2} (2.1 V, 0.25 A) with 0.5 Hz, 50% duty cycle (Supplementary Figs. 8a–c). However, no increase in neural activity was observed in the hippocampal CA3 region (Supplementary Figs. 8d–e). Our results confirm the feasibility of transcranial neural activation up to a depth of approximately 0.7 mm, including the skull thickness (approximately 0.2 mm), using the ReaChR virus and red LED.

Next, we measured neural activation using NIR light on the skull of a mouse infected with the ReaChR virus and injected with green UCPs. We observed a statistically significant increase in neural signals in the thalamus region when NIR light was applied at 275.5 mW·mm^{-2} (2.6 V, 0.25 A) with 0.5 Hz, 50% duty cycle (Supplementary Figs. 9a–c). Our results confirmed that transcranial neural activation was possible up to a depth of approximately 3 mm, accounting for skull thickness, using the ReaChR virus, NIR LED, and green UCPs.

Finally, we measured neural inhibition using NIR light on the skull of a mouse previously infected with the stGtACR2 virus and injected with blue UCPs. We observed a statistically significant decrease in neural signals in the thalamus with NIR illumination at 275.5 mW·mm^{-2} (2.6 V, 0.25 A) (Supplementary Figs. 10a–c). Our results confirmed the feasibility of transcranial neural inhibition up to a depth of approximately 3 mm, accounting for the skull thickness, using the stGtACR2 virus, NIR LED, and blue UCPs.

In conclusion, we successfully demonstrated transcranial neural modulation in vivo up to a depth of approximately 3 mm. Additionally, we expect that transcranial bimodal neuromodulation in vivo will be possible to a depth of approximately 0.7 mm without optical interference. This can be achieved by combining the ReaChR virus with a Red LED and the stGtACR2 virus with an NIR LED and Blue UCPs.

Evaluation of spatial resolution and stimulation control in transcranial optogenetic stimulation using UCPs

To precisely modulate specific brain functions or neural circuits, it is crucial to stimulate local brain regions with high spatial resolution. In this study, we evaluated the spatial resolution of transcranial optogenetic stimulation and the ability to control the stimulated region by varying the quantity of injected UCPs. To assess the stimulated region, we compared the number of c-Fos-expressing cells after stimulation with varying quantities of injected particles. Mice infected with the ReaChR virus were injected with 100, 400, or 800 nL of green-emitting UCPs and underwent optical stimulation outside the skull for 10 min (Fig. 2a). NIR light was applied at an intensity of 275.5 mW·mm^{-2} (2.6 V, 0.25 A), pulsing at 10 Hz with a 10 ms on-time duration (The details of the experimental protocol and analysis are provided in the Methods section). We observed a proportional increase in the number of c-Fos-positive cells with increasing particle volume, indicating expansion of the activated cell area (Fig. 2b–e). Specifically, c-Fos expression was observed in 9%, 15%, and 22% of the total cells in the groups injected with 100, 400, and 800 nL of particles, respectively (Fig. 2c and Supplementary Figs. 11 and 12). In contrast, only 3% of the cells expressed c-Fos in the control group, which did not receive virus or particle injections (Fig. 2c and Supplementary Figs. 12 and13). These results indicate that, under our experimental conditions, the effect of tNIRS alone was minimal, whereas the proportion of stimulated cells increased progressively with the quantity of particles injected.

Additionally, the average number of c-Fos positive cells per 40 μm-thick slice increased progressively with the injected volume, with 42 ± 28 cells for 100 nL, 66 ± 51 cells for 400 nL, and 142.8 ± 116 cells for 800 nL (Fig. 2f). We quantified the number of slices containing c-Fos-positive cells to estimate the spatial resolution of stimulation and stimulation ranges. The stimulation ranges were measured as 520 ± 40 μm for 100 nL, 600 ± 160 μm for 400 nL, and 1200 ± 200 μm for 800 nL, demonstrating a proportional increase with the injected volume of UCPs (Fig. 2e). Importantly, the spatial resolution achieved using our technique (approximately 0.5 mm) exceeds the roughly 1 mm resolution offered by transcranial focused ultrasound stimulation (tFUS), which was previously considered the most precise transcranial brain stimulation method (Supplementary Fig. 14)[29–31]. Additionally, the spatial resolution of our technique surpasses that attained by transcranial optogenetics (approximately 1 mm) using only high-sensitivity opsin[10]. Consequently, our findings suggest that both the stimulated range and the number of activated cells increase linearly with the quantity of injected particles, and the minimum spatial resolution (520 μm) offers superior resolution to that of existing transcranial brain stimulation techniques[29].

Motion control by multiple-site optogenetic neuromodulation

Through electrophysiological experiments utilizing a neural probe, we demonstrated the viability of our strategy for the transcranial modulation of neural activity in vivo. Subsequently, we assessed the possibility of behavioral control using the developed system in freely behaving animals. As a control, we evaluated the behavioral impact of LED irradiation on normal wild-type mice. After attaching the LED array to the skull above the left premotor cortex (M2) region, we observed the behavioral activity of the mice in response to the LED in the ON and OFF states in an open-field maze (as described in the Methods section). We found no differences in behavioral activity during the red and NIR LED on- and off-states (Supplementary Movie 2 and Supplementary Fig. 15). This suggests that the weight of the system and LED operation did not significantly affect the locomotor activity of the mice (Supplementary Fig. 2 and Supplementary Fig. 15).

Next, we assessed the feasibility of the motion control system by selectively stimulating multiple brain regions. Specifically, we targeted the M2 and superior colliculus (SC) regions, and immediate behavioral changes were observed upon stimulation. The M2 region has been associated with circling behavior[32,33], while the SC region has been linked to arrest behavior[34]. To activate the left and right M2 neurons, we utilized a combination of the ReaChR virus and red LEDs. To activate SC neurons located in a relatively deep region (~ 1.2 mm from the skull), we employed a combination of ReaChR virus, NIR LED, and Green UCPs.

After injecting the virus and particles into each region, two red LEDs and one NIR LED were attached to each injection site (Fig. 3a and Supplementary Figs. 16 and 17) as described in the Methods section. We anticipated three different behavioral changes upon selective stimulation of each region (e.g., left-circling behavior upon left M2 stimulation) (Fig. 3b). As expected, upon stimulation of the left M2 region using red light (10 Hz, 10 ms, 63 mW·mm^{-2} of light intensity) with our system, the mouse was observed to turn to the left (Fig. 3c and Supplementary Movie 3). By comparing the number of turns in each direction before and after stimulation, we confirmed a rapid increase in the number of turns to the left, demonstrating the selective stimulation of the left M2 region (Fig. 3c). Similarly, upon stimulation of the right M2 region using red light (10 Hz, 10 ms, 63 mW·mm^{-2} of light intensity), the mouse turned to the right (Fig. 3d and Supplementary Movie 3). The increase in the number of turns to the right confirmed selective stimulation of the right M2 region (Fig. 3d). Finally, upon stimulation of the SC region with NIR light (single pulse, 10 ms, 275.5 mW·mm^{-2} of light intensity), we observed that the mouse temporarily slowed down before returning to normal movement after a few seconds (Fig. 3e and Supplementary Movie 3).

Simulations were also conducted to evaluate the spatial resolution achievable with external light stimulation using a red LED. Prior to

https://doi.org/10.1038/s41467-024-54759-0

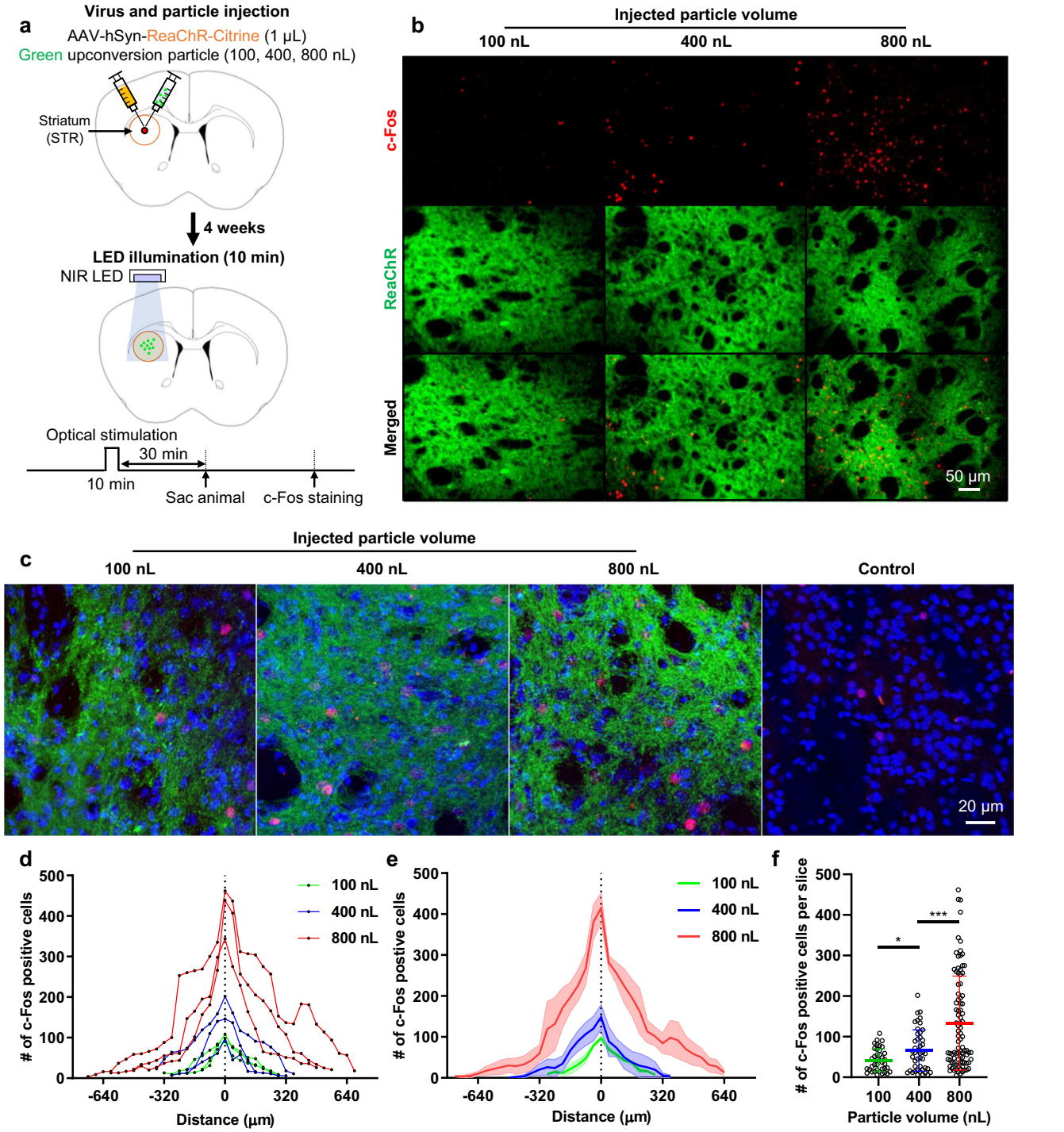

Fig. 2 | Spatial resolution of transcranial brain optogenetic method in vivo. **a** Schematic diagrams of virus/particle injection and experimental process. ReaChR virus was injected into striatum (STR). Green upconversion particles of varying quantities (100, 400, and 800 nL at a concentration of 20 mg·mL^{-1}) were injected into the same region. After 4 weeks, the c-Fos expression experiment was conducted. **b** The expression of c-Fos in the target region according to the quantities of the particles. **c** High magnification image of c-Fos expression. The control group consists of mice that underwent NIR stimulation without any injection of virus or particles. In the image, red represents c-Fos expression, green indicates ReaChR virus-infected neurons, and blue represents DAPI (labeling cell nuclei). **d** The number of c-Fos positive cells according to the volume of particles injected into individual mice. Three mice were used for each condition. Each data point represents the number of c-Fos positive cells in a 40-μm brain slice. **e** The number of c-Fos positive cells according to the volume of particles. The bold colored lines represent the mean value from the three mice. The lighter shade represents the standard error of the mean (SEM). **f** The number of c-Fos positive cells per slice according to the volume of particles (100 nL-400 nL: $t(82) = 2.616$, $p = 0.1057445$, 400 nL-800 nL: $t(134) = 3.708$, $p = 0.00030456$; $n = 39$ for 100 nL; $n = 45$ for 400 nL; $n = 91$ for 800 nL where n is the number of slices exhibiting c-Fos expression from three mice.). Statistical analysis was performed by the two-tailed unpaired t test, and $p < 0.05$ was considered significant. $^{*}p < 0.05$, $^{***}p < 0.001$. The c-Fos experiments were independently repeated in three mice with similar results to ensure reproducibility, and the representative images are shown in the figure.

https://doi.org/10.1038/s41467-024-54759-0

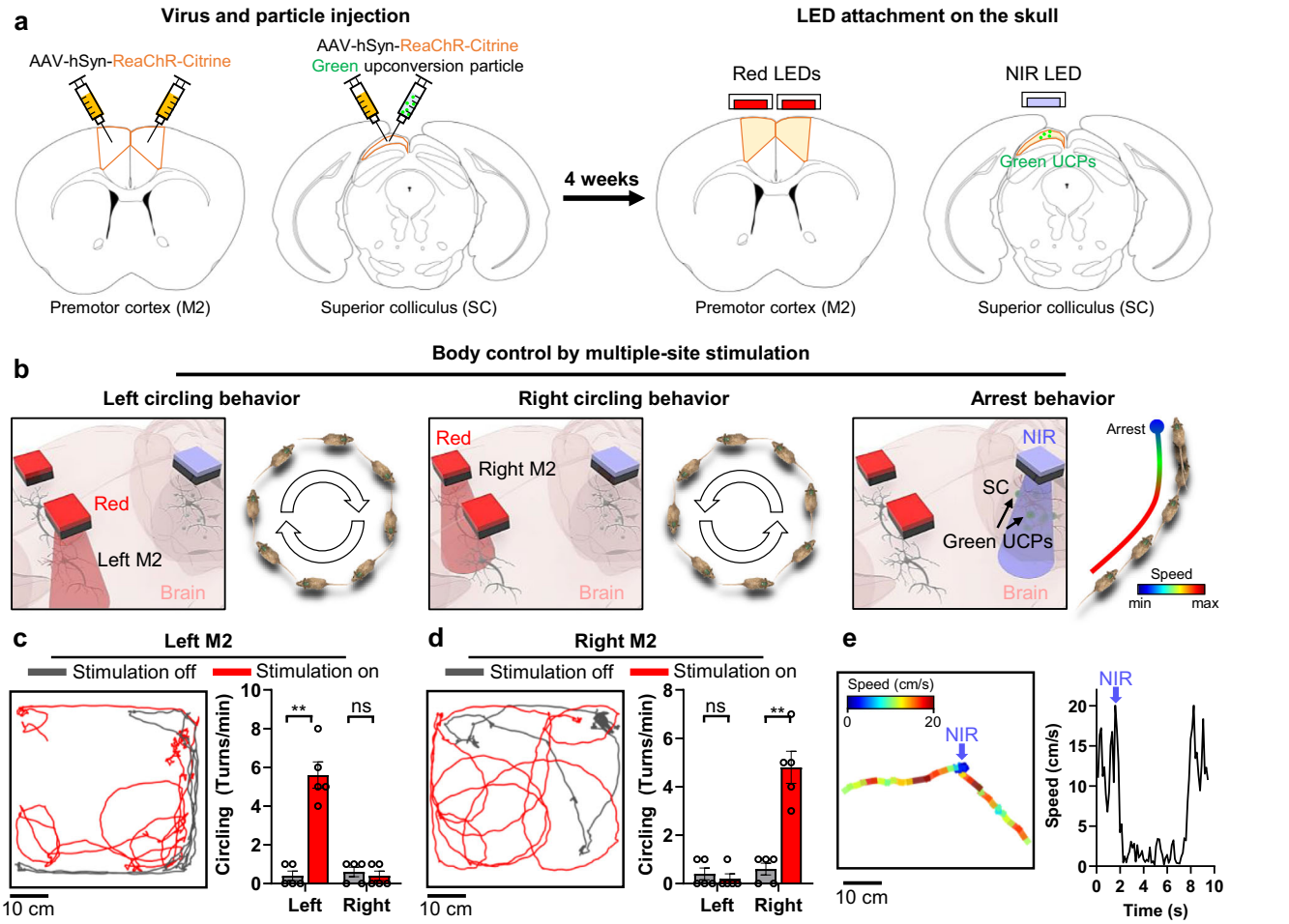

Fig. 3 | Selective, multi-site neuromodulation and monitoring of behavioral changes. a The schematic diagrams of virus/particle injection and LED attachment to the skull. ReaChR virus was injected into the left/right premotor cortex (M2) and superior colliculus (SC). The green upconversion particles were injected into the SC. After 4 weeks, two Red LEDs and one NIR LED were attached above the left/right M2 and SC regions. **b** Schematic diagrams for behavioral modulation (i.e., left/right circling behaviors (10 Hz, 10 ms ON time) and arrest behavior (1 time, 20 ms ON time)) by selective, multi-site neuromodulation. **c** Representative trajectory and comparison of the number of left or right circling behaviors per minute according to local neuromodulation off and on for left M2 neurons (Left: $p = 0.0079$, Right: $p > 0.9999$; $n = 5$ mice.). **d** Representative trajectory and comparison of the number of left or right circling per minute according to local neuromodulation off and on for right M2 neurons (Left: $p > 0.9999$, Right: $p = 0.0079$; $n = 5$ mice.). **e** Speed change by local neuromodulation of SC neurons. Blue arrow indicates the timing of NIR light on. The data are presented as mean values ± s.d. All statistical analyses were performed using the two-tailed Mann-Whitney test, and $p < 0.05$ was considered significant. $^{**}p < 0.01$. ns: no statistical significance.

the simulations, we measured the light dispersion angle of the red LED with the square thermal isolator attached to limit the light spread. These measurements were conducted in a dark environment, with distances ranging from 1 to 4 mm between the LED and a paper ruler (Supplementary Fig. 18a). We observed that the light spread ranged from 2, 3, 4, and 5 mm at distances of 1, 2, 3, and 4 mm, respectively (Supplementary Table 3). Using basic mathematical calculations, we determined that the light dispersion angle in air was approximately 53.14° (Supplementary Note. 2). Using this dispersion angle and the optical properties of the mouse skull and tissue for red light[17,35], we performed Monte Carlo simulations to evaluate light spread within the brain[36,37]. The simulations indicated that approximately 10% of the light reached a depth of 1.25 mm and extended laterally up to 0.75 mm at a depth of 1 mm (Supplementary Fig. 18b). Hence, the estimated spatial resolution of the light when targeting ReaChR-infected neurons was approximately 0.75 mm. To avoid overlap and crosstalk between the two light sources, a minimum separation of 1.5 mm would be necessary. In our behavioral experiments, we successfully achieved the expected effects by independently stimulating the left or right cortex (left M2 or right M2). This success was likely due to a larger population of neurons responding within the targeted region. Although the spatial resolution of our LED-based system has certain limitations, clear differences in the extent of stimulation and the number of responsive cells in adjacent areas allowed for successful selective behavioral modulation.

In conclusion, we successfully induced various behavioral changes in freely behaving mice through multiple-site transcranial stimulation using the developed system. This validates the potential for motion control through transcranial and multisite modulation.

Behavioral control by bimodal optogenetic neuromodulation

The combination of two different opsins enables the activation or inhibition of neural activity in a single brain region. To evaluate the functionality of bimodal optogenetic neuromodulation in freely behaving mice, we targeted the medial prefrontal cortex (mPFC) region because of its involvement in social competition[25,38]. The mPFC was chosen as the stimulation site because of its role in determining the outcome of competition; activation of mPFC neural activity leads to a win, whereas inhibition results in a loss[25]. For bimodal neuromodulation, we injected ReaChR, stGtACR2 viruses, and Blue UCPs into the mPFC (Fig. 4a and Supplementary Fig. 19). Red and NIR LEDs were attached to the injection site, and each mouse underwent individual

https://doi.org/10.1038/s41467-024-54759-0

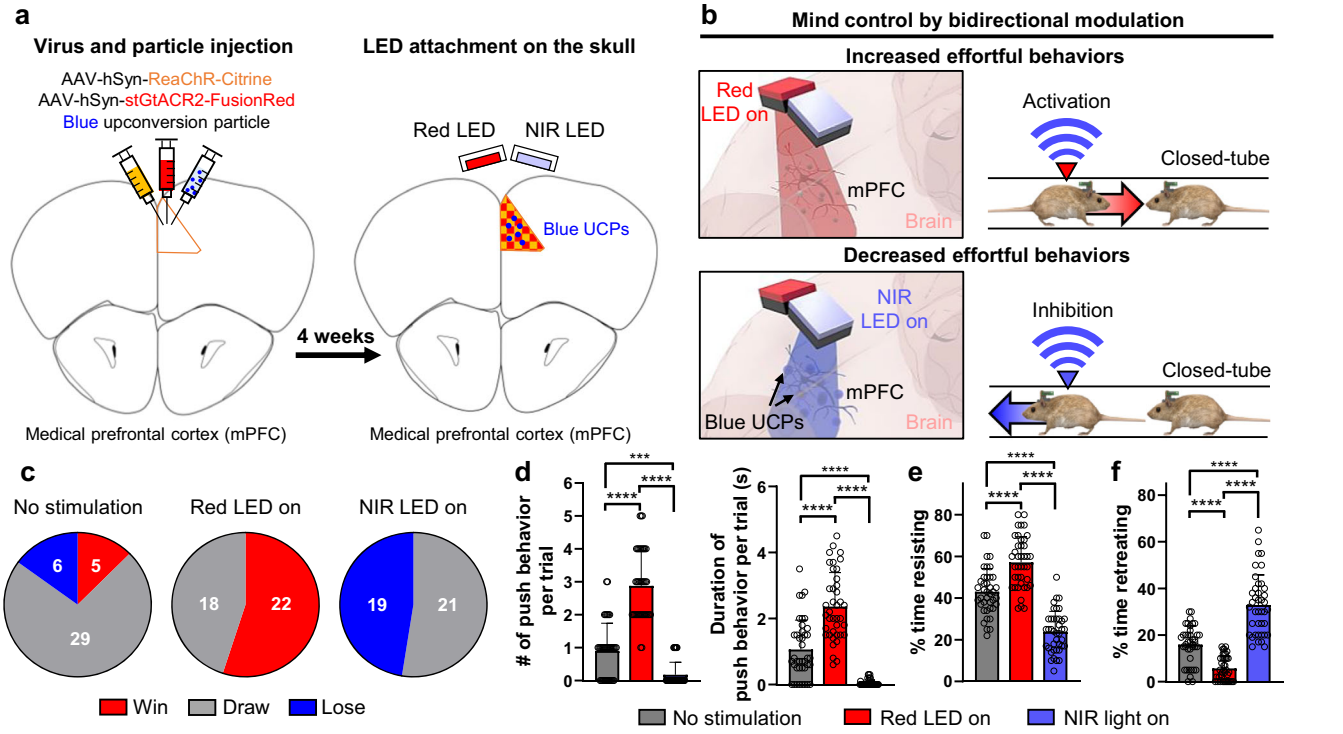

Fig. 4 | Bimodal neuromodulation and monitoring of effortful behavioral changes. a The schematic diagrams of virus/particle injection and LED attachment to the skull. ReaChR and stGtACR2 viruses and blue upconversion particles were injected into the medial prefrontal cortex (mPFC). After 4 weeks, Red and NIR LEDs were attached to the skull above the mPFC. **b** Schematic diagrams for behavioral control (i.e., effortful behavior) of the mouse by bimodal neuromodulation of the mPFC neurons in the closed-tube test. Activation of the mPFC neurons increased the effortful behavior when the Red LED was on. Inhibition of the mPFC neurons decreased the effortful behavior when the NIR LED was on. **c** Overall winning history of four mice (i.e., 40 trials) according to each stimulus condition (i.e., no stimulation, red LED on (10 Hz, 10 ms ON time), or NIR LED on (10 Hz, 10 ms ON time)) in the closed-tube test. One test consisted of 10 trials. **d** The number and the duration of push behavior per trial according to each stimulus condition (the number of push behavior per trial: $F(2,117) = 117.5$, $p < 0.0001$; the duration of push behavior per trial: $F(2,117) = 87.45$, $p < 0.0001$; $n = 40$ trials). **e** Percentage of time that mice resisted per trial according to each stimulus condition ($F(2,117) = 89.74$, $p < 0.0001$; $n = 40$ trials). **f** Percentage of time that mice retreated per trial according to each stimulus condition ($F(2,117) = 87.71$, $p < 0.0001$; $n = 40$ trials). The data are presented as mean values ± s.d. All statistical analyses were performed using one-way ANOVA with Tukey's multiple comparisons test, and $p < 0.05$ was considered significant. ***$p < 0.001$, ****$p < 0.0001$.

training in the closed-tube setup (Fig. 4a) (as described in the Methods section).

Well-trained mouse pairs were used in the closed-tube test. On the first day, no light was applied. On the second day, we either activated or inhibited mPFC neurons by applying red light (10 Hz, 10 ms, 63 mW·mm^{-2} of light intensity) or NIR light (10 Hz, 10 ms, 275.5 mW·mm^{-2} of light intensity) to one mouse (Fig. 4b and Supplementary Movie 4). After conducting the same experiment on four pairs of mice, we compared the competition results. In the absence of stimulation, the numbers of wins and losses were similar (Fig. 4c). However, the activation of mPFC neurons by the red LED resulted in a rapid increase in wins without any losses, whereas the suppression of mPFC neurons by the NIR LED led to a rapid increase in losses without wins (Fig. 4c). These results demonstrate successful control of competitive behavior through transcranial bimodal neuromodulation.

We also analyzed the behavior of mice in the closed-tube test, categorizing it into four sub-behaviors: push, resist, retreat, and other (as described in the Methods section). Activation of the mPFC by the red LED increased both the number and duration of push behaviors, whereas suppression by the NIR LED decreased push behaviors (Fig. 4d). Similarly, the duration of resistance increased during the red LED-on trials and decreased during the NIR LED-on trials (Fig. 4e). Conversely, retreat behavior decreased when the red LED was on and increased when the NIR LED was on (Fig. 4f). These results demonstrate that our system enables transcranial bimodal neuromodulation in freely behaving mice, allowing control of behavior-related cognitive functions in the closed-tube test.

Modulation of complex social behaviors in food competition test

This synergistic strategy for transcranial optogenetic methods enables precise transcranial brain modulation with multi-site and bimodal optogenetic neuromodulation. Additionally, we developed a wireless system to facilitate the simultaneous control of the brain activity in multiple mice. To demonstrate the utility of the system, a food competition test was performed, which is a complex social experiment performed between two mice (Fig. 5a) (The detailed experimental protocol, including surgery, experimental setup, and training, is provided in the Methods section). In this experiment, two mice ran to a food pellet contained in a square space. One mouse started eating the food pellet, and the competitive behavior of both mice was simultaneously controlled using the system (Fig. 5b). The NIR LED (10 Hz, 10 ms, 275.5 mW·mm^{-2} of light intensity) attached to the head of the mouse that reached the food pellet first was turned on to suppress competitive behavior by suppressing neural activities in mPFC region. Meanwhile, the red LED (10 Hz, 10 ms, 63 mW·mm^{-2} of light intensity) attached to the head of the other mouse was turned on to activate competitive behavior by activating neural activities in mPFC region, inducing competition and extortion for the food pellet by modulating the brain activities of both mice (Supplementary Movie 5). The results

https://doi.org/10.1038/s41467-024-54759-0

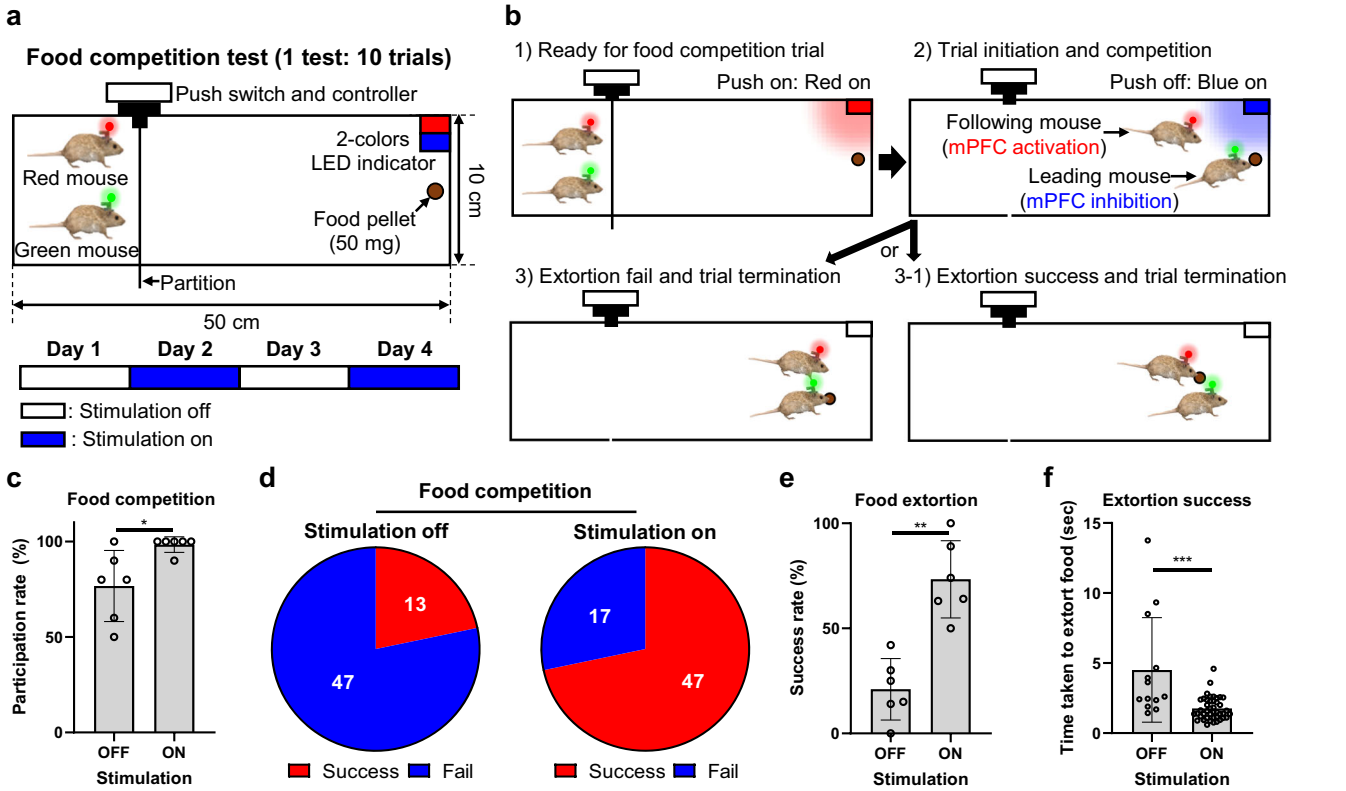

Fig. 5 | Modulation of extorting behaviors in food competition test. a Schematic illustration showing the experimental setup for the food competition test. One test consisted of 10 trials. The test was performed for 4 days. **b** Schematic illustrations showing the experimental protocol for one trial in the food competition test. **c** Comparison of participation rate according to stimulation off and on (10 Hz, 10 ms ON time) in 3 mice pairs ($p = 0.0281$; white circle: n = 6 tests per pair.). **d** The number of extortion success or fail according to stimulation off and on. **e** Comparison of success rate of food extortion according to stimulation off and on from 3 mice pairs ($p = 0.0022$; white circle: $n = 6$ tests per pair.). **f** Comparison of time taken to extort food according to stimulation off and on in extortion success trials ($p = 0.0001$; white circle: $n = 13$ (stimulation off) $n = 46$ where n is the number of successful extorting trials from 3 mice pairs.). The data are presented as mean values ± s.d. with individual data points. All statistical analyses were performed using the two-tailed Mann-Whitney test, and $p < 0.05$ was considered significant. $^{*}p < 0.05$, $^{**}p < 0.01$, $^{***}p < 0.001$. ns: no statistical significance.

showed a sharp increase in the participation rate in food competition during the stimulation-on trials (Fig. 5c and Supplementary Fig. 20). In addition, the number of successful food extortion trials increased (Fig. 5d–e and Supplementary Figs. 21 and 22). The time required to extort the food pellets also increased during the stimulation-on trials (Fig. 5f). In conclusion, the wireless system successfully controlled the competitive behavior of two mice simultaneously through transcranial brain modulation, demonstrating its potential for use in complex social experiments.

Reverting motor dysfunctions through the activation of neural activity in a mouse model of Parkinson's disease

One of the most important applications of TBS is the potential delivery of treatment protocols for various brain diseases. The developed wireless TBS system can serve as an effective tool for exploring treatment methods for brain diseases associated with motor dysfunction. Thus, we applied the developed system to relieve symptoms related to motor dysfunction in a mouse model of Parkinson's disease. Our goal was to reverse motor dysfunction by transcranially activating motor neurons related to motor function[39] (The detailed experimental protocol, including surgery, experimental setup, and induction of Parkinson's symptoms, is provided in the Methods section). Initially, we injected the ReaChR virus into the M2 region and green UCPs into the dorsomedial striatum (dmST) region to activate the M2 neurons and M2 axons (Fig. 6a). Our system utilizes two types of light sources and UCPs, enabling multiple stimulations using different light sources and UCP combinations. This dual-modality approach allows for the selective targeting of both M2 cell bodies and M2 axons, providing distinct contributions of somatic versus axonal activation in modulating motor functions. After allowing four weeks for sufficient infection, red and NIR LEDs were attached above the M2 and dmST regions for selective stimulation with different light sources (Fig. 6a). Following a one-week recovery period, Parkinson's symptoms were induced through continuous intraperiotoneal MPTP (1-methyl-4-phenyl-1,2,3,6-tetrahydropyridine) injection[40] (Fig. 6b). We confirmed that both the normal mice and LED-attached mice experienced a significant decrease in their behavioral activity following continuous MPTP injection compared to before the injection (Supplementary Movies 6-7 and Supplementary Fig. 23). In contrast, sham mice that were continuously injected with saline maintained similar activity levels (Supplementary Movie 8 and Supplementary Fig. 24). Thus, we confirmed the successful induction of Parkinson's disease symptoms through MPTP injection in virus-infected and LED-exposed mice. Subsequently, we stimulated M2 neurons and M2 axons of freely behaving mice in an open-field maze through transcranial M2 and dmST stimulation via red and NIR LEDs, respectively, with a frequency of 10 Hz and pulse duration of 10 ms (63 mW·mm^{-2} and 275.5 mW·mm^{-2} of light intensity from red and NIR LEDs, respectively) (Fig. 6c). We observed an increase in locomotor activity in all three mice during transcranial M2 and dmST stimulation (Fig. 6d–f and Supplementary Movie 9). Furthermore, we confirmed that the activation of the M2 neurons and M2 axons rescued motor functions, with a significant increase in both locomotor activity and speed (Fig. 5g–j). As a control experiment, we investigated whether NIR stimulation could affect motor activity in

https://doi.org/10.1038/s41467-024-54759-0

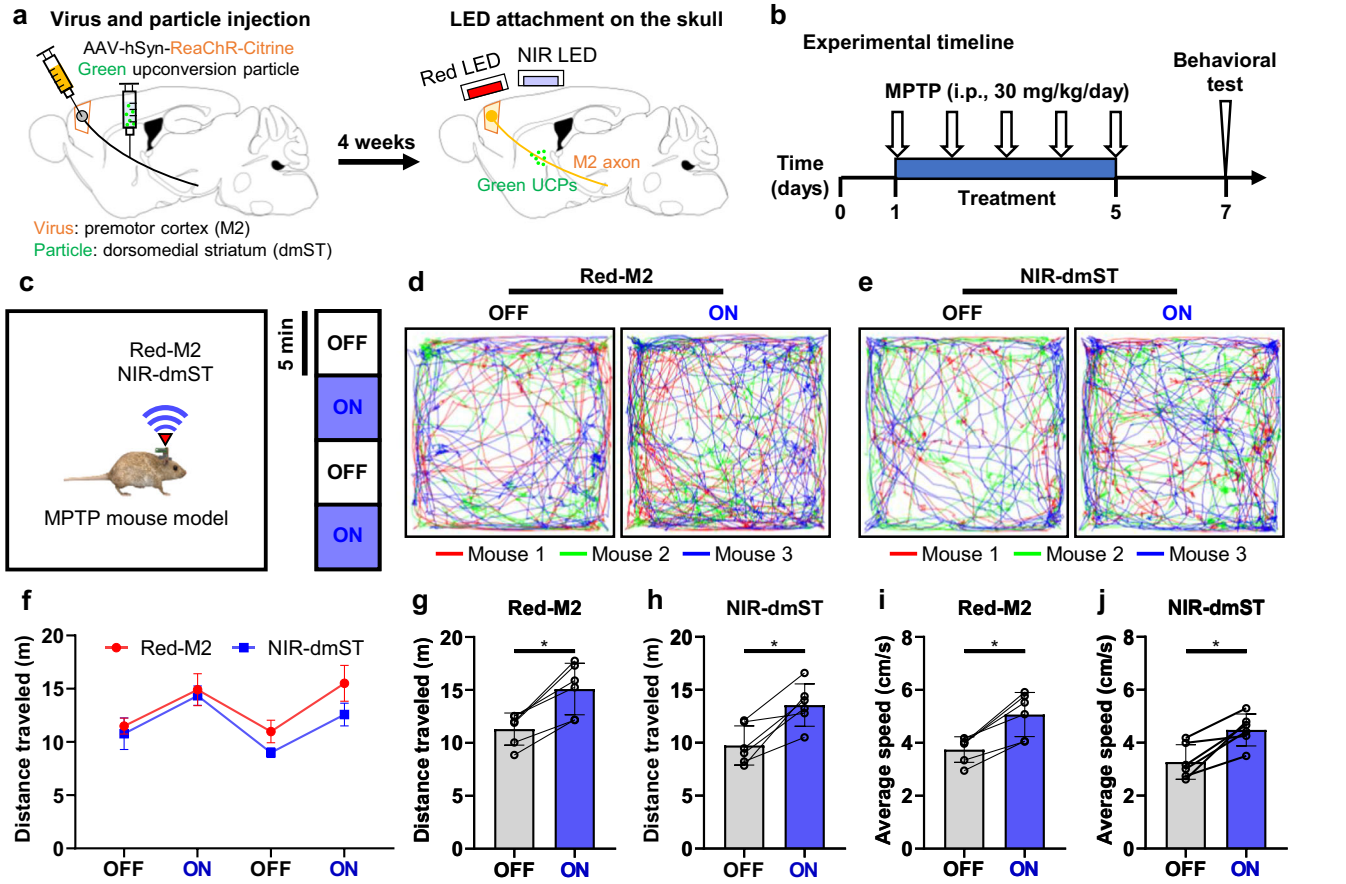

Fig. 6 | Alleviation of the behavioral deficit in MPTP-induced Parkinson's mice by precise modulation of M2 axons. a Schematic diagrams of virus/particle injection and LED attachment to the skull. ReaChR virus was injected into the premotor cortex (M2) region. Also, green upconversion particles were injected into the dorsomedial striatum (dmST) region. After 4 weeks, Red and NIR LEDs were attached above the M2 and dmST regions. **b** Experimental timeline showing the sequence of MPTP injection and behavioral tests. **c** Schematic illustration showing the experimental process. Testing for light delivery consisted of two cycles. One cycle consisted of two 5-minute epochs with alternating light delivery (OFF-ON). We operated the system with a 10 Hz frequency and a 10 ms ON time during the ON periods. **d** Trajectories of each mouse according to red LED on and off over the M2 region. The color of the line represents each mouse. **e** Trajectories of each mouse according to NIR LED on and off over the dmST region. The color of the line represents each mouse. **f** Distance traveled according to Red LED or NIR LED on and off during the experimental process. **g** Comparison of the distance traveled according to red LED on and off over the M2 region ($p = 0.0313$). **h** Comparison of the distance traveled according to NIR LED on and off over the dmST region ($p = 0.0313$). **i** Comparison of the average speed according to red LED on and off over the M2 region ($p = 0.0313$). **j** Comparison of the average speed according to NIR LED on and off over the dmST region ($p = 0.0313$). The data are presented as mean values ± s.d. with individual data points (white circle: $n = 6$ cycles. This experiment was conducted with three mice.). All statistical analyses were performed using the Wilcoxon matched-pairs signed rank two-tailed test, and $p < 0.05$ was considered significant. *$p < 0.05$.

MPTP-injected mice (a Parkinson's disease model) without genetic modifications or UCPs. MPTP injection significantly reduced the activity levels (Supplementary Movie 10 and Supplementary Figs. 25a, b), and NIR stimulation, applied using the same protocol, did not lead to increased activity in these mice (Supplementary Movie 11, Supplementary Figs. 25c–e, and Supplementary Fig. 26). These results suggested that the improvements observed in our experiments were specifically attributable to optogenetic modulation. Consequently, we successfully improved motor dysfunction in Parkinson's disease-induced mice through transcranial optogenetic neuromodulation using the system.

Discussion

We introduced and implemented a synergistic approach to achieve transcranial, multi-site, and bimodal neuromodulation in freely behaving animals. This method uses two transcranial optogenetic methods (highly sensitive opsins and UCPs) in conjunction with a wireless optoelectronic device. This approach enables simultaneous and precise behavioral modulation across multiple sites. Through in vivo electrophysiological experiments, we validated the effectiveness of transcranial neuromodulation and achieved a stimulation depth of approximately 3 mm, including the skull thickness, using three combinations of transcranial optogenetic methods: (1) ReaChR–Red LED, (2) ReaChR–NIR LED–Green UCP, and (3) stGtACR2–NIR LED–Blue UCP. Additionally, we achieved a spatial resolution of approximately 0.5 mm, surpassing that of previous transcranial brain stimulation techniques[10,29,30]. This superior spatial resolution enables more precise targeting of specific brain areas, marking a significant advancement in the field of transcranial brain stimulation. In particular, compared with tNIRS[6], our approach allows for localized, cell-type-specific stimulation within the regions in which the virus and UCPs have been injected. Furthermore, using a wireless optoelectronic device, we successfully controlled the behavior of mice in open-field and closed-tube tests. Our strategy allowed for unprecedented transcranial, multi-site, and bimodal neuromodulation in freely behaving mice. Furthermore, we applied this strategy in a complex social experiment involving food competition, effectively controlling competition between the mice and increasing their participation and success rates. Finally, we successfully alleviated decreased locomotor activity in a mouse model of Parkinson's disease through transcranial modulation using the system.

This strategy holds potential for various applications in neuroscience research, including complex behavioral and brain disease studies, by transcranially and precisely controlling brain circuits.

In future work, incorporating laser diodes (LDs) with superior directionality can significantly enhance system performance. Unlike LEDs, LDs provide distinct advantages such as higher directionality and improved power efficiency. LDs with high directionality can provide superior spatial resolution and enable the stimulation of deeper brain regions. Additionally, LDs can handle much higher power densities and maintain power conversion efficiencies of approximately 30%, making them ideal for experiments requiring concentrated and intense light[41]. Moreover, LDs do not experience an efficiency droop at higher power levels, which is a common issue with LEDs[41], making them more suitable for sustained high-power use. Therefore, integrating high-power LDs could extend the applicability of our approach from animal models such as mice to potential human applications.

Furthermore, our previous research indicated that mice exhibit minimal impact on activity levels with weights up to 5 g[26]. Given that our current device weighs <2 g, there is substantial room to increase the battery capacity without adversely affecting the behavior of the mice. Enhancing battery capacity is both feasible and critical for the success of long-term behavioral studies, as it would allow for extended operational times, effectively meeting the demands of such experiments.

Ultimately, we hope to utilize this strategy to treat brain diseases and enhance brain function in humans. However, certain limitations must be addressed prior to its application in humans. First, the limited stimulation depth (~ 3 mm) could limit its applicability in humans, necessitating advancements in light sources, such as LDs. Second, the need for intracranial surgery for viral and particle injections may limit accessibility, highlighting the importance of simpler surgical methods. A safe and simple surgical method is required to overcome this limitation, and the recent announcement by Neuralink of a surgical robot could be a solution[42]. Finally, ensuring the in vivo stability against viruses and particles is essential. Although some viruses for optogenetics have been created, the in vivo stability of the particles still needs to be verified, and the development of particles that can be safely verified in the body is required.

Despite these challenges, our study presents a highly effective strategy for precise transcranial brain modulation that combines transcranial optogenetic methods with a wireless optoelectronic device. In the short term, we anticipate that our approach will be used in various brain studies related to brain circuits and diseases, thereby enabling precise bimodal neuromodulation in freely behaving animals. In the long term, we hope that our strategy will play a key role in the treatment of brain diseases and enhancement of brain function in humans.

Methods

Packaging of the LED array

Small red and NIR LEDs (Red LED: XQERDO-H0-0000-000000701, Cree Inc, USA; NIR LED: SFH 4180S A01, OSRAM, Germany) were used in this study. The size of both LEDs is 1.6 mm × 1.6 mm. The active area of the LEDs is 1 mm × 1 mm for the Red LED and 0.75 mm × 0.75 mm for the NIR LED. Both LEDs were soldered onto a custom-printed circuit board (PCB) with metal pads on both sides. A thin, coated copper wire (0.09 mm, SBYC40, SME, Republic of Korea) was soldered to the opposite side of the PCB. After being cut to a length of approximately 1.5 cm, the wire was soldered to another custom PCB connected with a 1.27 mm pitch 5-pin header. The four wires connected to the cathode of the four LEDs were soldered to the center pin. To block the spread of light transmitted from the LED, a 1-mm high square piece with black color was fabricated using a 3D printer (Ultimaker 2 + , Ultimaker, The Netherlands). The piece had an inner size equal to the active area size of the red LED (1 mm × 1 mm) and an outer size equal to the LED size (1.6 mm × 1.6 mm). The fabricated pieces were attached to each LED using an instant adhesive (Loctite 401 liquid super glue, LOCTITE, Germany). The fabricated LED array was very light, weighing only 0.1 g. Additionally, the active area of each LED was very narrow at 1 mm × 1 mm, which made it suitable for simultaneous application to multiple regions of the mouse's brain.

Design and configuration of the wireless control module

We designed a lightweight wireless control module for operating each LED in freely-behaving mice. To simultaneously control each module in social experiments using multiple animals, we integrated a Bluetooth 4.0 communication embedded chip, which allowed remote control of each module without signal interference using an Android-based smartphone through the application provided by the manufacturer. In addition, to control individual LEDs, two dual SPST switch ICs were integrated. To supply stable power to the module and LED, a 3.3 V LDO regulator and pMOSFET were integrated. Also, to control the LED's operating frequency and pulse width, we integrated an oscillator IC. The set frequency and pulse width are changeable by soldering other resistors and capacitors. Below is information for each electronic part integrated with the module and a brief description (Supplementary Fig. 3).

- Bluetooth 4.0 communication embedded chip (FBL770BC, Firmtech, Republic of Korea): Enables wireless control of the LED without signal interference
- Dual SPST switch IC (TS3A4742DCNR, Texas Instruments, USA): Allows for selection of LED and the frequency (1 Hz or 10 Hz) and pulse width (5 Hz or 10 ms)
- 3.3 V LDO regulator (TPS73733DRVR, Texas Instruments, USA): Supplies stable power to the entire ICs
- pMOSFET (NTJD4152PT1G, On Semiconductor, USA): Controls LED operation and provides stable current supply to the LED
- Oscillator IC (LTC6991CBCB, Analog Devices, USA): Sets frequency and pulse width
- Other passive components (e.g., resistors and capacitors): Ensure stable operation of each IC.

Each component was soldered to a thin custom PCB with a 0.5 mm thickness. After soldering the ICs and passive components, this control module can be used directly through the Android application without downloading a separate program into the module. Through a compact design and minimal component integration, the total weight of the module is only 0.9 g, which is light enough to apply to small animals such as mice. The module is powered by a 30 mAh lithium polymer (Li-Po) battery and has a total weight of 1.9 g, including the weight of the battery (0.9 g) and the LED array (0.1 g). When the LED was continuously operated at 10% duty cycle (10 Hz, 10 ms) using the wireless control module, it could be operated for about 1 hour, which was sufficient time to perform most behavioral experiments, including in vivo tests in this study.

Optical power measurement

We used a photodetector (918D, Newport Inc., Irvine, CA, USA) in combination with an optical power meter (1936-R, Newport Inc., Irvine, CA, USA) to characterize the light output power from the LEDs. The end of the LED, coupled with the square piece (i.e., thermal isolator), was positioned near the photodetector to ensure accurate light intensity measurements. The fluctuation in output power was measured to be within ±0.002 mW, indicating stable light emission from the LED.

Thermal measurements of LED operation

To address the potential thermal issues associated with the high-power operation of LEDs, we employed a 10% duty cycle to prevent continuous temperature increases. Thermal measurements were

performed under various conditions, including constant LED operation, 10% duty cycle operation, and with and without the attachment of a plastic-based thermal isolator of thermal isolator used in the experimental setup.

A small PTC thermistor (NB-PTCO-001, Measurement Specialties) was attached to the measurement pad to monitor surface temperature (Supplementary Fig. 6a). We continuously tracked the changing resistance of the thermistor in real time and calculated the temperature using the formula provided in the datasheet. This setup enabled us to capture the maximum temperature under conditions closely mimicking the experimental setup, ensuring accurate assessments of the potential impact on brain tissue. Maximum temperature was recorded after 10 minutes of LED operation under each condition.

Ethics

Every animal experiment has been carried out following a protocol approved by an ethical commission.

Animal preparation

All of the procedures were approved by the Korea Institute of Science and Technology (KIST) in Seoul, Republic of Korea. Also, the procedures were conducted in accordance with the ethical standards stated in the Animal Care and Use Guidelines of KIST. Mice were provided by the animal facility in KIST. Adult male C57BL/6 J mice (8 weeks of age; average weight of 30 g) were used in this study. Five or six mice were housed in a cage that had a 12:12 light-dark cycle and the temperature and humidity of the animal facility were maintained at 22 ± 2 °C and 50 ± 5%. The number of mice used is specified for each experiment.

Virus and particle injection and LED attachment

We performed a craniotomy and injected AAV virus into the target region using 1 μL of AAV-hSyn-ReaChR-citrine (titer: 4.29×10^{13} GC·mL^{-1}; KIST virus facility, Seoul, Republic of Korea) or AAV-hSyn-stGtACR2-FusionRed (titer: 6.67×10^{13} GC·mL^{-1}; KIST virus facility, Seoul, Republic of Korea) via a conventional method[43]. We also injected blue- or green-emitting upconversion particles (UCPs) into the target region with 1 μL of blue- or green-emitting lanthanide microparticles (LMP; Shanghai Keyan Phosphor Technology, China) dispersed in saline (20 mg·mL^{-1}). The photon conversion efficiency of the blue-emitting UCP is 0.1%, while that of the green-emitting UCP is 0.38%[21]. After waiting for four weeks for sufficient virus infection, the mice were anesthetized with 4% isoflurane for induction and with 1.5% isoflurane using an isoflurane vaporizer (SurgiVet Classic T3 vaporizer, Smiths Medical, Inc., USA). After fixing the anesthetized mice on a stereotaxic instrument (David Kopf Instruments, USA), we attached the LEDs to the skull over the injection site using dental cement (Vertex Self Curing, Vertex Dental, Netherlands). The mice were allowed to recover for one week before being subjected to the experiments.

In the experiment for expression of c-fos, we injected ReaChR virus and green-emitting UCPs into the dorsal striatum (0.7; ±2; −2.95, AP; ML; DV, in millimeters from the bregma) region (Fig. 2a). To compare the number of activated cells and the range of stimulation according to the amount of particles, we injected 1 μL of virus was injected, and particles dispersed in saline (20 mg·mL^{-1}) of 100, 400, and 800 nL were injected into the target region. We waited for four weeks for sufficient virus infection before conducting the experiment.

In the electrophysiological experiment, we injected ReaChR or stGtACR2 viruses and blue- or green-emitting UCPs into the sensory cortex (-1.5; −1.25; −0.75, AP; ML; DV, in millimeters from the bregma), hippocampal CA3 (-1.5; −1.25; −2, AP; ML; DV, in millimeters from the bregma), and thalamus (-1.5; −1.25; −3, AP; ML; DV, in millimeters from the bregma) regions (Supplementary Fig. 7). We waited for four weeks for sufficient virus infection before conducting the experiment.

In the motion control experiment, we injected the ReaChR virus into the left/right premotor cortex (+ 1.1; ± 0.6; −1.25, AP; ML; DV, in millimeters from the bregma) and superior colliculus (-4; −0.75; −1.1, AP; ML; DV, in millimeters from the bregma) regions, respectively. We only injected the green-emitting UCPs into the superior colliculus region. For this setup, the two LEDs were placed closely side by side to enable localized, direct stimulation of adjacent regions, enhancing motion control precision.

In the behavioral control and food competition experiments, we injected ReaChR and stGtACR2 viruses and blue-emitting UCPs particles into the medial prefrontal cortex region (+ 2.6; +0.12; −1.5, AP; ML; DV, in millimeters from the bregma). To enable effective simultaneous stimulation, the LEDs were positioned facing each other at approximately a 30-degree angle, ensuring consistent light delivery to the target behavioral area.

In the behavioral experiment using Parkinson's disease-induced mice, we injected ReaChR virus into the premotor cortex region (+ 1.1; −0.6; −1.25, AP; ML; DV, in millimeters from the bregma) and green-emitting UCPs into the dorsomedial striatum region (+ 0.5; −1.5; −3.2, AP; ML; DV, in millimeters from the bregma).

Additionally, in experiments where only activation or inhibition was applied independently to separate regions, each LED was positioned directly above the respective target area to deliver light perpendicularly onto the skull.

After injecting viruses and particles in all behavioral experiments, we followed the rest of the experimental procedure, including LED attachment and waiting time for virus infection and recovery, according to the method described above.

Histology

After each experiment was completed, the mice were transcardially perfused with physiological saline followed by 4% paraformaldehyde (PFA) in 0.1 M PBS. After carefully removing the LED array from the skull, the brains were extracted and post-fixed in the 4% PFA solution for 24 hours. The fixed brains were then cut into 100-μm coronal sections using a vibrating microtome (VT1200S, Leica, USA) and mounted on cover slides. Brain images were captured using a confocal fluorescent microscope with a 5x and 20x objective lens (LSM 700, Carl Zeiss, Germany) to confirm virus and particle injection sites.

c-Fos staining and Immunohistochemistry

In anesthetized mice, after a 10-minute period of optical stimulation (NIR light, 10 Hz, 10 ms, 275.5 mW·mm^{-2} of light intensity), followed by a 30-minute delay, the brains were extracted and fixed using the same method as in Histology section. Subsequently, c-fos staining and immunohistochemistry were performed following a previously established method[44]. The brains were coronally sectioned at a thickness of 40 micrometers using a cryotome (CM300, Leica). The brain sections underwent a 1-hour incubation at 37 °C in primary antibodies. The primary antibody, an anti-c-Fos solution (1:500, #SC-52G, Santa Cruz Biotechnology, Inc., Dallas, TX, USA), was prepared in a PBS containing 3% BSA and 0.2% Triton X-100. Following the incubation, the sections were rinsed with PBS and then incubated with the secondary antibody, Alexa Fluor 647 conjugated to donkey anti-rabbit (1:500; #711-605-152, Jackson Immuno Research Inc., West Grove, PA, USA), in PBS with 3% BSA and 0.2% Triton X-100, maintained for 2 hours at room temperature. After washing away the secondary antibodies with PBS, the sections were embedded in a mounting medium, and images were subsequently obtained using a TCS SP8 microscope with dichroic/CS optics (Leica). The number of c-Fos positive cells in each slice was counted based on the virus-infected area (i.e., the region where citrine fluorescence was observed). The number of c-Fos positive cells was automatically calculated using analysis software. Additionally, to analyze the ratio of c-Fos-expressing cells relative to the total cell nuclei (DAPI), we used the particle count function in ImageJ (open-source software). Particles smaller than 5 μm were excluded from the analysis.

Electrophysiological experiment and neural signal analysis

To evaluate transcranial neuromodulation in vivo under various combinations of viruses, LED, and particles, we used a silicon-based neural probe integrated with 16 black Pt microelectrodes (14 ×14 μm^2) to measure neural activity by light. The neural probe was prepared using a previously reported method[38], with 16 recording electrodes spaced 40 µm apart on a single shank. The probe had a width of 128 µm and a thickness of 20 µm. The average impedance of the electrodes was 17 ± 1 kΩ at 1 kHz. Additionally, the LED was operated at 2.1 V and 0.25 A with a 0.5 Hz, 50% duty cycle. An external power supply was used for LED operation for these experiments as the mice were anesthetized. A small heatsink (9 ×9 x 5 mm^3) was attached to the LED to dissipate heat, and the LED was positioned 1-2 mm away from the skull due to the difficulty of attaching the LED directly to the skull with the probe implanted in the brain.

We performed stereotaxic surgery on mice under anesthesia with 0.5% urethane (400 $mg{\cdot}kg^{-1}$) administered by intraperitoneal injection. After positioning the anesthetized mice on a stereotaxic frame (Model 940 small animal stereotaxic instrument, David Kopf Instruments, USA), we removed the scalp and drilled the skull at the target site. We slowly inserted the neural probe into the sensory cortex, hippocampal CA3, and thalamus regions (-1.5; −1.25, AP; ML in millimeters from the bregma). After placing the neural probe in each target site, we measured the spontaneous neural activities. Neural signals were recorded using an RHD2132 amplifier connected to an RHD2000 Evaluation System (20$kS{\cdot}s^{-1}$ per channel, 300 Hz high pass filter, 6 kHz low pass filter, 16-bit ADC for spike recording; Intan Technologies, USA). After stabilization for 10 minutes, red or NIR light was delivered obliquely from outside the skull to the target site, with the LEDs turned on at the same power used in behavioral experiments. During transcranial optical stimulation (0.5 Hz, 50% duty cycle), we recorded neural signals for at least 5 minutes in each target site. The recorded neural signals were analyzed using a previously reported spike-sorting algorithm[45] and were expressed on a raster and bar plot for quantitative analysis of the change in neural activity by the light.

Open-field test

To evaluate the effects of the system's weight or drug injection (i.e., MPTP and saline) on behavior, we conducted the open field test (OFT)[46,47]. To explain in more detail, four C57BL/6 mice were placed in an opaque white chamber (50 cm × 50 cm × 40 cm) for 30 minutes, either after a recovery period or intraperitoneal injection of the drugs, and their behavioral movements were video-recorded using a Windows10 camera. The videos were analyzed using idTracker[48]. To evaluate the effect of LED activation on behavior, we conducted an additional OFT for 20 minutes with four C57BL/6 mice in the same chamber. The LED was turned on and off alternately for 5-minute intervals during the 20-minute test. We compared the distances traveled by the mice during LED-off and LED-on periods using data extracted through idTracker.

Motion control experiment in open-field test

To evaluate the behavioral changes induced by transcranial neuromodulation of multi-site regions (i.e., left/right premotor cortex and superior colliculus), we performed open-field maze experiments (50 cm × 50 cm x 40 cm) with four virus- and particle-injected mice. Each mouse underwent three open-field tests (OFTs), and during each OFT, we turned on one LED to observe behavioral changes induced by neural activation in one brain region. We conducted each OFT with a time interval of at least 2 hours between each session. Each OFT was performed for a total of 10 minutes, where no stimulation was applied for the first 5 minutes, and stimulation was applied by turning on one LED for the remaining 5 minutes. For OFTs that induce left/right circling behaviors, we turned on the LED with a 10% duty cycle (10 Hz, 10 ms). In tests that induce arrest behavior, we manually turned on the LED for 20 ms while walking randomly. In the circling behavior test, we counted the number of turns in each direction before and after stimulation and compared and analyzed the results quantitatively. In the arrest behavior test, we observed the change in speed just before and after stimulation.

Simulation of light distribution within the brain

To estimate the light distribution from the red LED within the brain for optical stimulation, we utilized Monte Carlo simulations (Monte Carlo eXtreme; MCX)[36,37]. In the simulation, we modeled the skull and brain tissue using a domain size of 250 × 250 × 250 with 0.1 mm voxels.

For the skull (250 × 250 x 25 of domain size), we applied an absorption coefficient of 0.6 mm-1, a scattering coefficient of 2.5 mm-1, an anisotropy factor of 0.92, and a refractive index of 1.36[49]. For brain tissue (250 ×250 x 225 of domain size), we used an absorption coefficient of 0.4 mm^{-1}, a scattering coefficient of 4 mm^{-1}, an anisotropy factor of 0.92, and a refractive index of 1.36[50]. These parameters were chosen to accurately represent the optical properties of both the skull and brain tissues under red light illumination.

The light source was positioned at voxel (125, 125, 0) with a dispersion angle of 53.14°. A total of 1.96×10^{17} $photons{\cdot}ms^{-1}$ were emitted from the light source, reflecting the optical power of the red LED. This setup allowed us to evaluate the light intensity and spread across the cortical regions.

Behavioral control experiment in closed-tube test

To evaluate behavioral change using transcranial bimodal neuromodulation, we performed a closed-tube test with four pairs of mice based on a previously reported method[51]. The tests were conducted in an acrylic tube (30 cm × 3 cm × 5 cm) in an activity box. A Full HD camera was installed in front of the chamber to record the competition between the mice. We paired mice of the same age that were grown in separate cages to prevent unilateral winning in the test. The mice were starved for a day and trained in the chamber for two successive training days. With the system mounted, each mouse was trained to enter the tube and exit through the opposite end for 10 trials. The test was conducted over two days. On the first day of the test, there was no stimulation, and a total of 10 trials were performed. Pairs of mice were entered at the two inlets of a tube and met in the middle. We designated the mouse that retreated first outside from the tube as the loser. On the second day, we applied either red light or NIR light (10 Hz, 10 ms ON time) to one mouse using the system. Thus, a total of 20 trials were performed on the second day, with 10 trials using red light and 10 trials using NIR light delivered to the mouse. We counted and compared the number of wins and losses of mice for each trial (no stimulation, red-light stimulation, and NIR-light stimulation). We also classified observed behaviors into four sub-behaviors (i.e., push, resist, retreat, and others) by referring to a previously reported study[25] and comparatively analyzed each behavior by stimulus condition.

Behavior definitions and annotations in closed-tube test

We classified the behaviors observed in the closed-tube test into distinguishable categories by referring to a previously reported study[25]. The behavior categories and their definitions in this test are as follows:

- Push: Behavior of pushing the opponent back out of the closed-tube.
- Resist: Behavior of resisting the opponent's push.
- Retreat: Behavior of retreating from the opponent's push.
- Others: Behaviors other than the above behaviors, such as stillness without pushing each other or self-sniffing.

The behaviors of the mice were manually annotated frame by frame through video analysis. The videos were reviewed in detail by an observer who did not participate in the experiment, using a 50-millisecond scale.

Food competition test

To evaluate the feasibility of the system in a complex social experiment, we conducted a food competition test in an acrylic chamber (50 cm × 10 cm x 30 cm) in the activity box, based on previous studies[26,38]. The chamber was divided into two zones by a square opaque acrylic plate. The starting zone was 10 cm × 10 cm, and the competition zone was 40 cm × 10 cm in size. The acrylic plate was inserted into the groove of the chamber to divide it into two zones and pressed the push switch. The push switch controlled the state of the RGB LED array connected to the controller (Arduino Pro mini 328, Arduino.cc, Italy). When the push switch was on, the red light turned on, and when the push switch was off by removing the acrylic plate, the green LED light turned on for 5 seconds. The mice learned the rule through the LED's status. Two mice were placed in the starting zone, and a small food pellet of 45 mg (F0165, Bio-Serv, USA) was placed at the end of the competition zone. When the acrylic plate was removed, the food competition proceeded with the green LED turned on. The two mice ran for food, and the competition ended when the food ran out. We defined this procedure as one trial, and 10 trials were performed per day per mice pair.

To prevent unilateral winning in the food competition, mice of the same age, grown in different cages, were paired. The mice were adapted to the small food pellet (45 mg) during the 1-week calorific restriction period, during which their weight was maintained at 85-90% before the calorific restriction. Each mouse was trained in the same chamber during this period. The training was conducted in the same way as the food competition test, but with no competitors. Individual training was conducted for 5 trials.

After individual training, we performed the food competition test for 4 days. The test was conducted in 10 trials per day. On the first and third days, the test was performed on both mice without stimulation. On the second and fourth days, the test was performed while stimulation was applied to the two mice by turning on the LED (10 Hz, 10 ms ON time) during the competition. NIR light was applied to the mice that arrived first to induce inhibition of mPFC neurons, and red light was applied to the mice that followed to induce activation of mPFC neurons. Accordingly, competition was urged in the following mice to extort the food pellet easily.

Induction of Parkinson's disease and behavioral test

To evaluate the feasibility of the system in animals with brain disease, we targeted a mouse model with Parkinson's disease. For inducing Parkinson's disease symptoms, we used MPTP (1-methyl-4-phenyl-1,2,3,6-tetrahydropyridine), which is commonly used in mouse models to induce Parkinson's disease symptoms[40]. We injected MPTP (30 mg·kg^{-1}) daily through intraperitoneal injection for 5 days, following a previously reported study[40]. Due to the toxicity of MPTP, all injection procedures were performed in a fume hood. We provided sufficient water and food to the cage in the fume hood during the injection period, and we maintained a 12:12 light-dark cycle, as well as the same temperature and humidity as the animal facility. The control group, consisting of saline-injected mice, followed the same procedure in the same hood. To ensure there was no residual MPTP in the hood, normal mice of the same age were injected with saline in the same hood seven days after it was thoroughly cleaned. After confirming a decrease in behavior due to the induction of Parkinson's symptoms through MPTP injection, the mice were used in behavioral tests seven days after the injection (Fig. 6b). In the behavioral test, we conducted the OFT for 20 minutes with three Parkinson's disease-induced mice in an opaque white chamber (50 cm × 50 cm × 40 cm). For 20 minutes, the LED turned on and off alternately for 5 minutes (10 Hz, 10 ms ON time). We compared the traveled distances and speed during the LED-off and LED-on periods based on data extracted through idTracker.

Statistical analysis

The statistical analyses were performed using GraphPad Prism (GraphPad, USA). The normality of distribution of all statistically analyzed data was assessed by GraphPad Prism. If normality was met, the statistical analyses were performed by parametric analysis (e.g., two-tailed t-test). If normality was not met, the statistical analyses were performed by non-parametric analysis (e.g., Mann-Whitney test). Additionally, all statistical analyses were based on independent samples. The specific statistical test used for each set of data is included in the legend of each figure.

Reporting summary

Further information on research design is available in the Nature Portfolio Reporting Summary linked to this article.

Data availability

All data supporting the findings of this study are available within the article and its supplementary files. Any additional requests for information can be directed to, and will be fulfilled by, the corresponding authors. Source data are provided with this paper.

Code availability

The signal analysis for this study was performed using Matlab. Also, the code used for the spike-sorting process is available at https://doi.org/10.1038/s41467-019-11628-5.

References

1. Polania, R., Nitsche, M. A. & Ruff, C. C. Studying and modifying brain function with non-invasive brain stimulation. *Nat. Neurosci.* **21**, 174–187 (2018).
2. Boes, A. D. et al. Noninvasive brain stimulation: challenges and opportunities for a new clinical specialty. *J. Neuropsychiatry Clin. Neurosci.* **30**, 173–179 (2018).
3. O'Connell, N. E., Marston, L., Spencer, S., DeSouza, L. H. & Wand, B. M. Non-invasive brain stimulation techniques for chronic pain. *Cochrane Database Syst. Rev.* **4**, CD008208 (2018).
4. Schulz, R., Gerloff, C. & Hummel, F. C. Non-invasive brain stimulation in neurological diseases. *Neuropharmacology* **64**, 579–587 (2013).
5. Vosskuhl, J., Struber, D. & Herrmann, C. S. Non-invasive brain stimulation: a paradigm shift in understanding brain oscillations. *Front Hum. Neurosci.* **12**, 211 (2018).
6. Nizamutdinov, D., Ezeudu, C., Wu, E., Huang, J. H. & Yi, S. S. Transcranial near-infrared light in treatment of neurodegenerative diseases. *Front Pharm.* **13**, 965788 (2022).
7. Lin, J. Y., Knutsen, P. M., Muller, A., Kleinfeld, D. & Tsien, R. Y. ReaChR: a red-shifted variant of channelrhodopsin enables deep transcranial optogenetic excitation. *Nat. Neurosci.* **16**, 1499–1508 (2013).
8. Kim, S. et al. Non-invasive optical control of endogenous Ca(2+) channels in awake mice. *Nat. Commun.* **11**, 210 (2020).
9. Gong, X. et al. An ultra-sensitive step-function opsin for minimally invasive optogenetic stimulation in mice and macaques. *Neuron* **107**, 38–51.e38 (2020).
10. Chen, R. et al. Deep brain optogenetics without intracranial surgery. *Nat. Biotechnol.* **39**, 161–164 (2021).
11. Chen, S. et al. Near-infrared deep brain stimulation via upconversion nanoparticle-mediated optogenetics. *Science* **359**, 679–684 (2018).
12. Liu, X. et al. Near-infrared manipulation of multiple neuronal populations via trichromatic upconversion. *Nat. Commun.* **12**, 5662 (2021).
13. Zhang, F. et al. Multimodal fast optical interrogation of neural circuitry. *Nature* **446**, 633–639 (2007).

14. Boyden, E. S., Zhang, F., Bamberg, E., Nagel, G. & Deisseroth, K. Millisecond-timescale, genetically targeted optical control of neural activity. *Nat. Neurosci.* **8**, 1263–1268 (2005).
15. Kim, C. Y. et al. Soft subdermal implant capable of wireless battery charging and programmable controls for applications in optogenetics. *Nat. Commun.* **12**, 535 (2021).
16. Lee, J. et al. Rapidly-customizable, scalable 3D-printed wireless optogenetic probes for versatile applications in neuroscience. *Adv. Funct. Mater.* **30**, https://doi.org/10.1002/adfm.202004285 (2020).
17. Yang, Y. et al. Wireless multilateral devices for optogenetic studies of individual and social behaviors. *Nat. Neurosci.* **24**, 1035–1045 (2021).
18. Gutruf, P. et al. Fully implantable optoelectronic systems for battery-free, multimodal operation in neuroscience research. *Nat. Electron.* **1**, 652–660 (2018).
19. Taal, A. J. et al. Optogenetic stimulation probes with single-neuron resolution based on organic LEDs monolithically integrated on CMOS. *Nat. Electron.* **6**, 669–679 (2023).
20. Li, L. et al. Colocalized, bidirectional optogenetic modulations in freely behaving mice with a wireless dual-color optoelectronic probe. *Nat. Commun.* **13**, 839 (2022).
21. Zhang, Z., Han, Q., Lau, J. W. & Xing, B. Lanthanide-doped upconversion nanoparticles meet the needs for cutting-edge bioapplications: recent progress and perspectives. *ACS Mater. Lett.* **2**, 1516–1531 (2020).
22. Mahn, M. et al. High-efficiency optogenetic silencing with soma-targeted anion-conducting channelrhodopsins. *Nat. Commun.* **9**, 4125 (2018).
23. Park, J. et al. A wireless, solar-powered, optoelectronic system for spatial restriction-free long-term optogenetic neuromodulations. *Sci. Adv.* **9**, eadi8918 (2023).
24. Park, S. I. et al. Stretchable multichannel antennas in soft wireless optoelectronic implants for optogenetics. *Proc. Natl Acad. Sci. USA* **113**, E8169–E8177 (2016).
25. Zhou, T. et al. History of winning remodels thalamo-PFC circuit to reinforce social dominance. *Science* **357**, 162–168 (2017).
26. Yoon, Y. et al. Neural probe system for behavioral neuropharmacology by bi-directional wireless drug delivery and electrophysiology in socially interacting mice. *Nat. Commun.* **13**, 5521 (2022).
27. Lee, E. et al. Enhanced neuronal activity in the medial prefrontal cortex during social approach behavior. *J. Neurosci.* **36**, 6926–6936 (2016).
28. Owen, S. F., Liu, M. H. & Kreitzer, A. C. Thermal constraints on in vivo optogenetic manipulations. *Nat. Neurosci.* **22**, 1061–1065 (2019).
29. Yang, D., Shin, Y. I. & Hong, K. S. Systemic review on transcranial electrical stimulation parameters and eeg/fnirs features for brain diseases. *Front Neurosci.* **15**, 629323 (2021).
30. Mosilhy, E. A. et al. Non-invasive transcranial brain modulation for neurological disorders treatment: A narrative review. *Life Sci.* **307**, 120869 (2022).
31. Rezayat, E. & Toostani, I. G. A review on brain stimulation using low intensity focused ultrasound. *Basic Clin. Neurosci.* **7**, 187–194 (2016).
32. Montgomery, K. L. et al. Wirelessly powered, fully internal optogenetics for brain, spinal and peripheral circuits in mice. *Nat. Methods* **12**, 969–974 (2015).
33. Wu, Y. et al. Wireless multi-lateral optofluidic microsystems for real-time programmable optogenetics and photopharmacology. *Nat. Commun.* **13**, 5571 (2022).
34. Liang, F. et al. Sensory cortical control of a visually induced arrest behavior via corticotectal projections. *Neuron* **86**, 755–767 (2015).
35. Ghanbari, L. et al. Craniobot: A computer numerical controlled robot for cranial microsurgeries. *Sci. Rep.* **9**, 1023 (2019).
36. Fang, Q. & Boas, D. A. Monte Carlo simulation of photon migration in 3D turbid media accelerated by graphics processing units. *Opt. Express* **17**, 20178–20190 (2009).
37. Fang, Q. Mesh-based Monte Carlo method using fast ray-tracing in Plucker coordinates. *Biomed. Opt. Express* **1**, 165–175, (2010).
38. Shin, H. et al. Interference-free, lightweight wireless neural probe system for investigating brain activity during natural competition. *Biosens. Bioelectron.* **195**, 113665 (2022).
39. Magno, L. A. V. et al. Optogenetic Stimulation of the M2 Cortex Reverts Motor Dysfunction in a Mouse Model of Parkinson's Disease. *J. Neurosci.* **39**, 3234–3248 (2019).
40. Fornai, F. et al. Parkinson-like syndrome induced by continuous MPTP infusion: convergent roles of the ubiquitin-proteasome system and alpha-synuclein. *Proc. Natl Acad. Sci. USA* **102**, 3413–3418 (2005).
41. Wierer, J. J., Tsao, J. Y. & Sizov, D. S. Comparison between blue lasers and light-emitting diodes for future solid-state lighting. *Laser Photonics Rev.* **7**, 963–993 (2013).
42. Musk, E. & Neuralink. An Integrated Brain-Machine Interface Platform With Thousands of Channels. *J. Med. Internet Res.* **21**, e16194 (2019).
43. Lowery, R. L. & Majewska, A. K. Intracranial injection of adeno-associated viral vectors. *J. Vis. Exp.* https://doi.org/10.3791/2140 (2010).
44. Yang, S. H. et al. Neural mechanism of acute stress regulation by trace aminergic signalling in the lateral habenula in male mice. *Nat. Commun.* **14**, 2435 (2023).
45. Shin, H. et al. Multifunctional multi-shank neural probe for investigating and modulating long-range neural circuits in vivo. *Nat. Commun.* **10**, 3777 (2019).
46. Tatem, K. S. et al. Behavioral and locomotor measurements using an open field activity monitoring system for skeletal muscle diseases. *J. Vis. Exp.* 51785, https://doi.org/10.3791/51785 (2014).
47. Seibenhener, M. L. & Wooten, M. C. Use of the Open Field Maze to measure locomotor and anxiety-like behavior in mice. *J. Vis. Exp.* e52434, https://doi.org/10.3791/52434 (2015).
48. Perez-Escudero, A., Vicente-Page, J., Hinz, R. C., Arganda, S. & de Polavieja, G. G. idTracker: tracking individuals in a group by automatic identification of unmarked animals. *Nat. Methods* **11**, 743–748 (2014).
49. Haleh, S., Hirac, G. & Frederic, P. Optical properties of mice skull bone in the 455- to 705-nm range. *J. Biomed. Opt.* **22**, 10503 (2017).
50. Mesradi, M. et al. Experimental and analytical comparative study of optical coefficient of fresh and frozen rat tissues. *J. Biomed. Opt.* **18**, 117010 (2013).
51. Wang, F. et al. Bidirectional control of social hierarchy by synaptic efficacy in medial prefrontal cortex. *Science* **334**, 693–697 (2011).

Acknowledgements

This work was supported by the Research program for understanding and regulation of brain function of the National Research Foundation (NRF) funded by the Ministry of Science & ICT (NRF-2022M3E5E8081196 (I.-J.C.)) and the Bio & Medical Technology Development Program of the National Research Foundation (NRF) funded by the Ministry of Science & ICT (RS-2024-00441103 (I.-J.C.)). This work was also supported by the Korea Evaluation Institute of Industrial Technology (RS-2024-00419956 (I.-J.C.)) and Korea University intramural grant.

Author contributions

H.S. performed most of the experiments, analyzed the data, prepared the figures, and wrote the manuscript. M.-H.N., S.E.L., S.H.Y., E.Y., J.T.J., and H.K. were involved in the in vivo experiments. J.W. and Y.C. were involved in preparing the in vivo experiments. Y. Y. was involved in the characterization of the system. I.-J.C. discussed the results, provided comments, and wrote the manuscript. All of the authors reviewed the manuscript.

Competing interests
The authors declare no competing interests.

Additional information
Supplementary information The online version contains supplementary material available at https://doi.org/10.1038/s41467-024-54759-0.

Correspondence and requests for materials should be addressed to Il-Joo Cho.

Peer review information *Nature Communications* thanks Xing Sheng, and the other, anonymous, reviewer(s) for their contribution to the peer review of this work. A peer review file is available.